

Special-Purpose Quantum Processor Design

Bin-Han LU^{1,2}, Yu-Chun WU^{*1,2}, Wei-Cheng KONG³, Qi ZHOU^{1,2}, and Guo-Ping GUO^{†1,2,3}

¹Key Laboratory of Quantum Information, Chinese Academy of Sciences, School of Physics, University of Science and Technology of China, Hefei, Anhui, 230026, P. R. China

²CAS Center For Excellence in Quantum Information and Quantum Physics, University of Science and Technology of China, Hefei, Anhui, 230026, P. R. China

³Origin Quantum Computing Company Limited, Hefei 230026, China

Abstract

Full connectivity of qubits is necessary for most quantum algorithms, which is difficult to directly implement on Noisy Intermediate-Scale Quantum processors. However, inserting swap gate to enable the two-qubit gates between uncoupled qubits significantly decreases the computation result fidelity. To this end, we propose a Special-Purpose Quantum Processor Design method that can design suitable structures for different quantum algorithms. Our method extends the processor structure from two-dimensional lattice graph to general planar graph and arranges the physical couplers according to the two-qubit gate distribution between the logical qubits of the quantum algorithm and the physical constraints. Experimental results show that our design methodology, compared with other methods, could reduce the number of extra swap gates per two-qubit gate by at least 104.2% on average. Also, our method's advantage over other methods becomes more obvious as the depth and qubit number increase. The result reveals that our method is competitive in improving computation result fidelity and it has the potential to demonstrate quantum advantage under current technical conditions.

INTRODUCTION

In recent years, quantum computing has progressed to a “Noisy Intermediate-Scale Quantum(NISQ) era” in which quantum processors have dozens to hundreds of noisy qubits [1–3]. NISQ processors have short coherence time and quantum operations with nonzero error rates [4]. Besides, only a subset of physical qubit pairs are coupled for two-qubit gates, i.e., the Physical Coupling Graphs(PCG) of NISQ processors are not complete. Here, the vertexes of the PCG are physical qubits and the edges are physical couplers. Quantum algorithms are represented by a quantum circuit model. In general, quantum circuits allow two-qubit gates to act on any qubit without restriction. Therefore, a transformation process that insert extra swap gates before two-qubit gates between uncoupled physical qubits to move the qubits to coupled qubits is required. Because swap gate consists of imperfect gates supported by NISQ processors, this process will significantly decrease the computation result fidelity [5].

To improve the fidelity, two solutions are proposed, one is finding the optimized transformation process on the fixed PCG to reduce extra swap gates [6–23]. The other is designing the PCG according to a weighted Circuit Coupling Graph(CCG) of the quantum circuit. Here the vertex of CCG is logical qubit and the edge weight is the number of successive two-qubit gate blocks [24]. Since the designed PCG is more suitable for the given CCG, the transformation process adds less swap gates than on fixed PCG. The commonly used PCGs are two-dimensional(2d) lattice graphs because they can be used in Quantum Error Correction(QEC) [25–28] and fabricating these structures on superconducting system is technically practicable [30,31]. In [24], the authors proposed a method that designs the PCG based on 2d lattice graph.

However, under current technology, NISQ processor has too few qubits to perform fault-tolerant universal quantum algorithms [22]. Therefore, making quantum processor into lattice

graphs is not necessary in the NISQ era. As the general CCG is not a lattice graph, we can extend PCG from lattice graph to general planar graph. Actually, in [4,32,33], we know that manufacturing the general planar PCG is also feasible.

In this paper, we propose a Special-Purpose Quantum Processor Design(SPQPD) method. The method extends PCG from lattice-graph to general planar graph. We first get the CCG of the circuit, and then arrange the physical couplers according to the CCG under physical constraints. Finally, we get a manufacturable PCG. When using realistic algorithms [48] as circuit benchmarks, we find that compared with other methods, our method, on average, reduces the extra swap gate number by at least 104.2%. To further verify the effectiveness of SPQPD, we use a series of random circuits as benchmarks and carry out the control variable experiments. When fixing qubit number, the number of extra gates in our method decreases as depth increases while other methods either increase or have no obvious trend; when fixing algorithm depth, the growth rate of extra gates to the qubit number is reduced at least by 37.1%. The results reveal that the PCG designed by SPQPD outperforms its competitors. Hence, it has great potential to demonstrate the quantum advantage in the NISQ era.

If quantum processor has enough qubit resources for QEC, i.e., transformation won't reduce the fidelity of the computation results, SPQPD method can still play an important role because it can reduce the number of swap gates, the depth of the circuits, and the time of quantum algorithm execution effectively.

RESULTS

Technical Constraints of Manufacturable PCG

There are some technical constraints to NISQ processor's PCG structure.

Maximum degree The essence of the two-qubit gate is to entangle the control and target qubits [34–37]. In superconducting system, the physical coupler that create entanglement

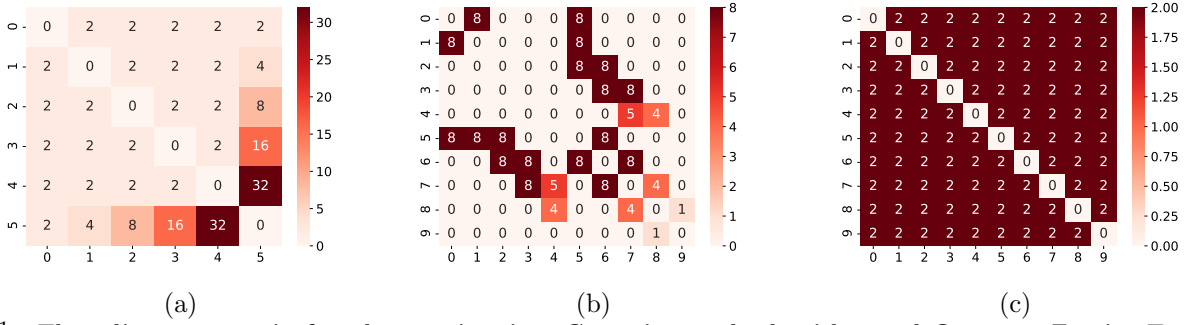


Figure 1: **The adjacency matrix for phase estimation, Grover’s search algorithm and Quantum Fourier Transformation(QFT).** (a) It can be seen that almost all of the high connection weight is concentrated on vertex q_4 . (b) The connection is on the off-diagonal, the adjacency matrix forms a chain-like structure. (c) All edges have the same weight.

will interfere the working frequency of the qubit [32, 33, 38–41]. Thus fabricating entangled structure is non trivial. There is a fully entangled structure [42] and the largest number of entangled qubits so far is 10. But its drawback is that the entanglement cannot be closed, which will create difficulties in the control of larger-scale quantum processor. Therefore, the current architecture still tends to establish entanglement between two qubits. Limited by the state of the art, the number of couplers on one qubit can’t be too large, i.e., there is a maximum degree of vertex in PCG. In this paper, the maximum degree is set to be 6 because the largest degree of 2d lattices [44] and the achievable highest degree of structures in [24] are 6.

Planarization Fabricating the 2d superconducting quantum processor is a mature technology [30, 31]. Thus all qubits and couplers are placed on one layer and the couplers cannot cross each other in space. In the future, when multi-layer processor is available, some qubits or couplers can be placed on another layer. In this situation, for the couplers on the same layer, circuit transformation is still of great essential [45, 46] and SPQPD can play a significant role. For this reason, a legitimate PCG should have a way of embedding to 2d plane without edge-interaction except at vertexes, i.e., the PCG should be a planar graph.

Profiling the Coupling Information

To design the quantum processor, we should profile information about the quantum circuit. The number of two-qubit gates between vertexes pair is the key information to bridge the quantum circuit and processor, because there are a large number of two-qubit gates in a circuit while NISQ processor has extremely limited coupler resources. Designing a quantum processor according to the number of two-qubit gates is expected to dramatically reduce the number of extra gates. For this reason, two-qubit gates information should be profiled.

Fig. 1 are three examples of profiling the coupling information of a quantum circuit. These examples indicate the existence of different CCG patterns. Fig. 1(a) is an example of the phase estimation algorithm. Most of the weight is concentrated between q_4 and other vertexes. Fig. 1(b) is an example of Grover’s search algorithm. The matrix elements are concentrated on the off-diagonal, thus the corresponding CCG forms a chain-like structure. Fig. 1(c) is an example of the Quantum Fourier Transformation(QFT) algorithm. All edges are equally weighted.

Fig. 1 illustrates that the quantum processors can be customized for different circuits. E.g., the q_4 in fig. 1(a) need more coupler resources, PCG of fig. 1(b) should be designed as a chain structure and the coupler resources in fig. 1(c) should be arranged more uniformly.

Pruning

The second step is pruning the edges. After profiling, we get a CCG. Since the CCG often violates the constraints, fabricating quantum processor with the original CCG’s structure is intractable. Pruning some edges will reduce the degree, eliminate the intersections and make the CCG meet the constraints. To answer the question that which edges need to be pruned, we present the following facts.

First, if the edge is pruned, the two-qubit gates between the corresponding vertexes cannot execute directly, and swap gates are required. Second, since the weight is the number of two-qubit gates, pruning the edges with smaller weight can reduce the number of extra swap gates. Third, the vertex connected to more edges with larger weight should have more coupler resources. Finally, the pruned graph must be planarizable.

Hence in this section, our goal is to modify the CCG into a planar graph with only a few important vertexes with high degree. It is sparser than the original CCG, more flexible and maybe more similar to the original CCG than the PCG with lattice-graph structures. And a PCG that meets the constraints and is as similar to the original CCG as possible can be designed in the further step.

Ranking Vertexes

Here, we rank the vertexes according to their importance. The key idea of our method is giving more coupler resources to the more important vertex. Because the connection information(detail discussions are in the “METHODS” section) such as degree and weight of the connected edges of each vertex are different, it is natural to infer that the importance of vertexes is different. We define a metric of vertex importance in the “METHODS” section. Under the metric, if the edges connected to the less important vertex were pruned, fewer swap gates will be inserted in the transformation process.

Fig. 2 is an example design process from original CCG to the final legitimate PCG. This CCG is generated from a circuit provided by [48]. The sum of the edge weight connected to q_6 is greater than that of other’s, so it is an important vertex that needs more coupler resources. After the ranking subroutine, the ranking result is $q_6, q_7, q_5, q_3, q_0, q_4, q_2, q_1$.

Pruning Based on the Media Vertexes

Now we should complete the pruning process according to the ranking result. Based on the ideas proposed above, we shouldn’t change the vertexes with high rankings, but prune the edges of the vertexes with lower rankings.

The original CCG fig. 2(a) violates the constraint of planarization, thus the pruning subroutine is needed. The ranking result shows that the most important and the second impor-

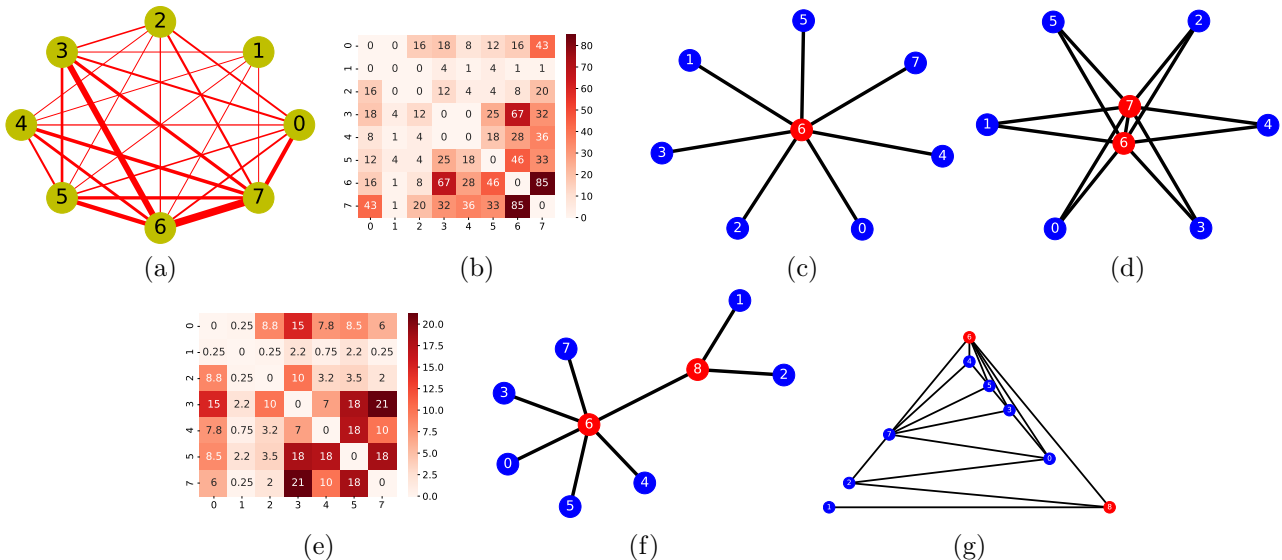


Figure 2: **Example of the whole PCG design.** (a) The original CCG. (b) The corresponding adjacency matrix of (a). (c) Pruning result of $N = 1$. (d) Pruning result of $N = 2$. (e) Interaction matrix I . (f) Result of splitting the media vertex and weight allocation. (g) The final CCG which is also a legitimate PCG.

tant vertex are q_6 and q_7 . Fig. 2(c) is the pruning result of the media vertex number $N = 1$, where q_6 is chosen as media vertex. Fig. 2(d) is the result of $N = 2$, where q_6 and q_7 are both chosen as media vertexes. These media vertexes are not only the most important, but also serve as the path to execute the two-qubit gate between non adjacent vertexes. After choosing the media vertexes, the edge that connect q_i, q_j is pruned if $\{q_i, q_j\} \cap \text{media_vertex_set} = \emptyset$, where media_vertex_set is the set of media vertexes. The pruned edges are stored in a *recover_set* that is useful in the ‘‘Recovering’’ section. The question of how many media vertexes should be selected is discussed in the ‘‘METHODS’’ section.

Handling the High Degree Vertex

Splitting the High Degree Vertex

The third step is handling the vertexes whose degree violate the maximum degree constraint. After pruning, although we have eliminated the intersections in the CCG and pruned some edges that violate degree constraint, the degrees of the media vertexes in the graph may still violate the constraint of the maximum degree. For this reason, the third step of SPQPD is adding ancilla vertexes and changing the media vertex v into a graph called media structure composed of multiple vertexes $\{v_1, v_2, \dots, v_n\}$. The logical qubit contained by the media vertex v now corresponds to one vertex v_i in media structure at a time. We connect a part of edges of media vertex to the ancilla vertexes to reduce the excessive degree. Fig. 3(a) and fig. 3(b) are two examples of reducing degree by adding ancilla qubits.

This step is defined as splitting media vertex. The media structure must satisfy the following four conditions. First, the media structure should be a connected graph. Therefore, for a media structure with n vertexes, the number of edges e of the media structure should satisfy $e \geq n - 1$. Second, as in fig. 3(a), from the external perspective of the media structure, media structure is a black box that behaves like the media vertex. Therefore, media structure should contain sufficient free connections for the non-media vertexes connected by the media vertex, i.e., $k \leq Dn - e$, where D is the maximum degree, k is the number of non-media vertexes connected by original me-

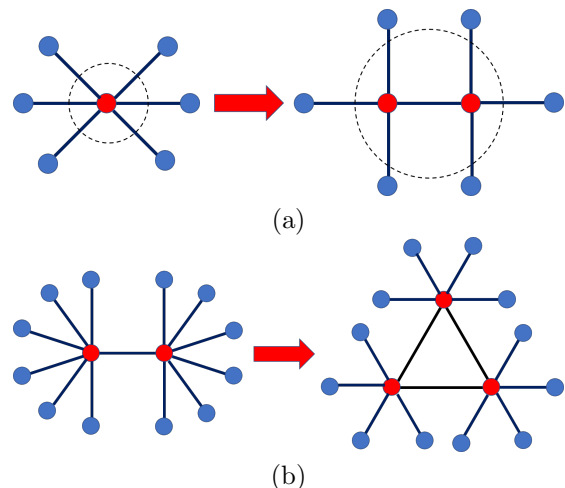


Figure 3: **Add ancilla qubits and change the media structure into a structure with multiple vertexes.** (a) The degree is reduced from 6 to 4. (b) The degree is reduced from 7 to 4.

dia vertex. Third, the graph of media structure should meet the technical constraints for manufacturable PCGs. Forth, the number of vertexes n should be as few as possible because increasing the number of ancilla qubits will increase the difficulty of processor manufacturing. The subroutine which can search for media structures based on these conditions will be discussed in the ‘‘METHODS’’ section.

Allocating the Non-Media Vertexes

After replacing the media vertex by media structure, we need to reconnect the non-media vertexes to the vertexes in the media structure. This step is called weight allocation and the allocation way is not unique. We should find an optimized allocation way to minimize the extra swap gates because of the following reasons.

First, because only one vertex v_i in the media structure contains the logical qubit of the original media vertex v at a time, swap gates are required if v_i doesn’t directly connected to the non-media vertex q_l when two-qubit gate g between q_l, v need to be executed immediately. To describe this, we define a matrix S whose element is the sum of the number of the two-qubit gate blocks in two subcircuits only about vertexes q_m, v and q_l, v .

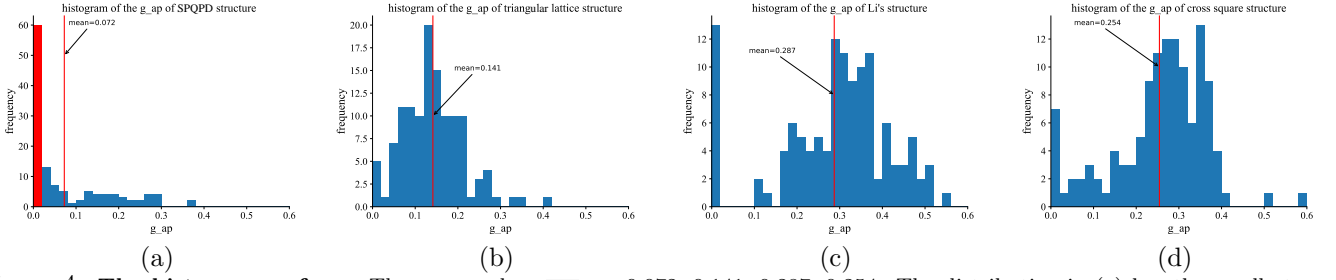


Figure 4: **The histograms of g_{ap} .** The mean values $\overline{g_{ap}}$ are 0.072, 0.141, 0.287, 0.254. The distribution in (a) has the smallest mean value. The red bar in (a) has the largest frequency and it belongs to the smallest interval.

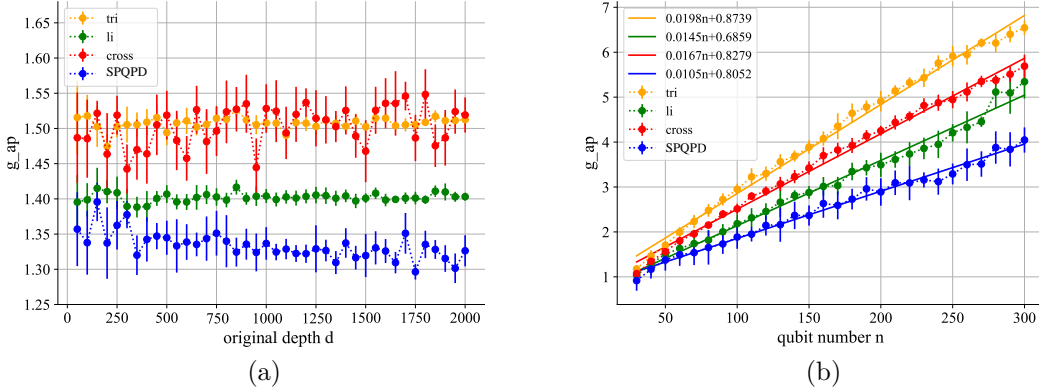


Figure 5: **The relationships between g_{ap} and original depth and qubit number.** (a) The relationship between g_{ap} and original depth. SPQPD method has the smallest g_{ap} within the depth range [50, 2000]. For SPQPD, the mean value of each error bar $\langle g_{ap} \rangle_d$ decreases as circuit depth gets larger. For the others, the corresponding character either increases or has no obvious trend. The qubit number is set to be 50. (b) The relationship between g_{ap} and qubit number. SPQPD method has the smallest g_{ap} growth rate among all structures, where original depth is set to be 200.

Second, the non-media vertex are now connected by media vertex, swap gates are required when two-qubit gate between non-media vertexes q_m, q_l need to be executed. The farther they are on the graph, the more swap gates are required. The adjacency matrix M can be used to describe this.

To describe how close q_m, q_l should be allocated on the media structure, we define an interaction matrix I whose element is $I_{ml} = aM_{ml} + (1-a)S_{ml}$, where a is the combination coefficient.

Another matrix required is C whose element is the shortest length between vertexes in media structure. Our goal is to find an allocation map $alloc$ to let the score

$$F = \sum_{ij, alloc[i]alloc[j]} C_{ij} I_{alloc[i]alloc[j]}, \quad (1)$$

$$alloc : V \rightarrow 2^{\{q|q \in \text{neighbor of } v\}} \quad (2)$$

get the minimum value, where $alloc$ is a map that allocates the neighbor of media vertex v to the vertexes in the media structure. V is the set of vertexes in media structure and v is the original media vertex.

In fig. 2(c), we set $N = 1$, the most important vertex is q_6 . Thus after the pruning subroutine, q_6 is selected as media vertex. q_6 violates the degree constraint and need to be replaced by a media structure. First, we try the media structure with two vertexes q_6, q_8 which meets the condition $1 = e \leq Dn - k = 6 \times 2 - 7 = 5$. Then, the non-media vertexes are allocated according to the matrix I . In fig. 2(e), the elements in columns 3, 5, 7, 0 and 4 of I is relatively larger than columns 1 and 2, thus allocating the former 5 vertexes to the same vertex q_6 will let the summation terms in eq. (1) with larger $I_{alloc[i]alloc[j]}$ become zero and reduce the value of F . After q_6 reaching the

degree constraint $D_{q_6} = 6$, q_1 and q_2 have to be allocated to q_8 , because they have less interaction with the former vertexes, the impact that their allocation is far away from the former important vertexes is smaller. Thus, the result is eq. (3), eq. (4) and fig. 2(f).

$$alloc[q_6] = \{q_5, q_0, q_3, q_7, q_4\}, \quad (3)$$

$$alloc[q_8] = \{q_1, q_2\}, \quad (4)$$

where q_6, q_8 are vertexes in media structure and the others are the non-media vertexes needed to be allocated.

The media vertexes with more than two vertexes have multiple non-isomorphic topological structures. In this case, we should repeat the process above and find the structure with the smallest score F .

Recovering

The fourth step recovering is to reconnect some pruned edges to the CCG. In fig. 2(f), vertexes except for q_6 are far from the maximum degree, this means that some edges in the *recover_set* can be recovered to the CCG. Based on the idea that changing the subgraph with smaller weight and degree has less impact, the edge with larger degree has higher recovery priority.

Fig. 2(g) is the final CCG of the routine. The structure of this CCG meets the constraints mentioned above, so it is also a legitimate PCG structure that can be implemented by the superconducting system.

Comparing the Number of Extra Swap Gates

Using 158 Benchmarks

Finally, we use a series of circuits as benchmarks to test SPQPD method and compare it with other lattice-graph struc-

tures. 158 circuits are used for the experiment [48]. Triangular lattice structure, the 2d planar lattice structure that with the largest degree 6 [44], structures designed by the method in [24] and cross square lattice structure based on the same foundation as the Li's structure are used as representatives of lattice-graph structures.

We define the metric as the number of extra swap gates per input two-qubit gate $g_{ap} = \frac{g_{add}}{g_{ori}}$ where g_{add} is the number of extra swap gates and g_{ori} is the number of original two-qubit gate.

Fig. 4(a)-(d) are the histograms of g_{ap} for four kinds of structures. The results show that on average, the SPQPD method has the best performance and its average $\overline{g_{ap}} = 0.072$. It is improved by 104.2% compared with the second-best structure, the triangular lattice structure. In fig. 4(a), a majority part of g_{ap} belongs to the smallest interval, which means that the SPQPD method can design the most suitable processor for a quantum algorithm.

Using Random Circuits

To further verify the effectiveness of SPQPD method, we evaluate its performance to circuits with different qubit numbers and depth. Random circuits within the desired qubit number and depth range are generated for such evaluation.

Since NISQ processor has dozens to hundreds of qubits, we set the range of qubit numbers to be [30, 300]. In [53], the order of the coherence time is in [10, 200] μ s and the gate execution time satisfies $t_{gate} > 10$ ns. Based on the data and the noise model in [32], if we choose $T = 100\mu$ s, $t_{gate} = 20$ ns, for a circuit with depth $d = 2000$, after rough calculation, the fidelity of computation result is less than 70%. At this depth, the fidelity is very low, thus the circuit depth won't exceed a few thousand and we set the range of depth to be [50, 2000].

Fig. 5(a)-(b) are the relationships between g_{ap} between qubit number and circuit depth. For error bars of fig. 5, we sample 100 random circuit outputs. Error bars are obtained by computing the credible intervals for the data set of circuits with the same size. These intervals are computed with normal distribution, with a credible level of 95%. This ensures that the mean value is inside the credible interval with a probability of at least 95%.

In fig. 5(a), if we consider the mean value $\langle g_{ap} \rangle_d$ of every data bar of circuits with depth d , the structures designed by the SPQPD method has the smallest $\langle g_{ap} \rangle_d$. To find out the trend of $\langle g_{ap} \rangle_d$ as depth increases, we use the Mann-Kendall trend test [50]. After computation, the statistics Z_c for SPQPD, triangle structure, Li's structure, and cross square structure are -3.92, -0.12, 0.59, and 2.81. Therefore, at the significance level $\alpha = 0.05$, the SPQPD method has an decreasing trend, cross square structure increasing and the other two have no obvious trend. This result reveals that the SPQPD method has good scalability for depth.

In fig. 5(b), the g_{ap} increases as the qubit number increases. Using linear regression, the slope of the SPQPD method is the smallest one 0.0105. The growth rate of SPQPD method is improved by 37.1% compared with the second-best method, Li's method.

In summary, all results show that the SPQPD method can design the most suitable planar quantum processor for quantum algorithm. It is an effective way to reduce the number of extra gates and improve the computation fidelity. As the scale of the algorithm expands, the structure designed by the SPQPD method's advantage becomes more obvious over other structures.

DISCUSSION

To improve the quantum computation fidelity, instead of following the old paths of optimizing the transformation process or designing quantum processor with lattice-graph structures, we come up with an idea that designing the quantum processor with general planar graph structures according to the quantum algorithm. In particular, we formalize our SPQPD method with four steps: profiling two-qubit gate information, pruning edges of unimportant vertexes, handling the high degree vertexes, and recovering the edges with large weights. The numerical experiments show that SPQPD method is a competitive alternative approach to improve the computation fidelity when executing quantum algorithms on NISQ processor. Therefore, the SPQPD method has great potential to demonstrate the quantum advantage in the NISQ era.

In conclusion, this work explores a step in mitigating the quantum software-hardware gap and provides a new idea for the development of special-purpose quantum processor. With the development of technology, SPQPD method might be used in the design of larger NISQ processor and multi-layer processor. Even after fault-tolerant quantum computation is realized, the SPQPD method will still have practical significance. PCG designed for certain CCG can reduce the number of swap gates and the circuit depth and therefore result in decreasing the execution time of quantum algorithms.

METHODS

Profiling Subroutine

We ignore all single-qubit gates, initialization, and measurement operations, and combine the two-qubit gates which act on the same two qubits successively. The reason for combining is that if the current map allows the first gate to be executed directly, then there is no need for more swap gates for the successive two-qubit gates. Therefore, in the circuit transformation process, they can be seen as a whole block. After counting the number of two-qubit gate blocks, we get the adjacency matrix M and the corresponding CCG.

Fig. 6 shows the process of information profiling. In fig. 6(a), after ignoring the one-qubit gates and measurement operations, we find that the two CNOT gates between q_0 and q_1 can be combined as one two-qubit block. The other CNOTs are two-qubit blocks themselves. Fig. 6(b) is the adjacency matrix of the circuit, whose element with index m, l represents the number of two-qubit gate blocks between q_m and q_l . Fig. 6(c) is the corresponding CCG of fig. 6(b). The relative width of the edges represents the relative size of the weight.

Vertex Ranking Subroutine

At first, we need to define some concepts about the connection information of the vertexes.

Definition 1 *The total weight of vertex q_m , $W_m = \sum_l M_{ml}$, representing the sum of total two-qubit block number of a vertex.*

Definition 2 *Weight dispersion of vertex q_m , c_m , representing the deviation of the number of two-qubit blocks the vertex executes with each of its neighbors.*

Based on the definitions and the discussion above, we choose the following three indicators to evaluate the importance of vertexes.

Vertex degree D_m , the larger the degree of the vertex is, the more important the vertex is.

Total weight, according to def. 1, the larger the total weight, the more frequently this vertex executes two-qubit gates with its neighbors, and thus more important the vertex is.

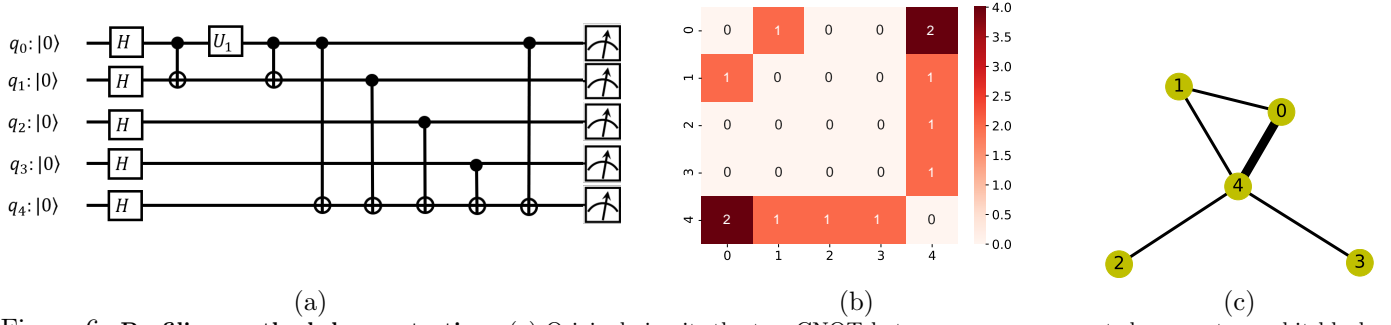


Figure 6: **Profiling method demonstration.** (a) Original circuit, the two CNOT between q_0, q_1 are counted as one two-qubit block. (b) The adjacency matrix of (a), whose element M_{ml} is the number of two-qubit blocks between q_m, q_l . (c) Corresponding CCG of (b), the relative width of the edges represents the relative size of the weight.

Weight dispersion, the smaller the weight dispersion, the more important this vertex is. The reason why we introduce this indicator will be discussed in the Recovering Subroutine.

Vertexes are sorted by these three indicators in **lexicographic order**.

Pruning Subroutine

The first step is choosing the top N most important vertexes as media vertexes. The second step is pruning the edges on the graph that don't connect to the media vertexes. The third step is storing those pruned edges to a *recover_set*.

Media Structures Searching Subroutine

We search for all candidate media structures that are not isomorphism with each other with n vertexes and delete those violate the constraints. n is searched from small to large within this range $[2, \infty]$. If legitimate media structures are found with n vertexes, the searching process stops immediately. Because the greater the number of ancilla qubits, the more difficult it is to manufacture the quantum processor. All of these media structures with n vertexes will be stored and be used as candidate media structures in the following "Weight Allocation Subroutine" subsection.

Weight Allocation Subroutine

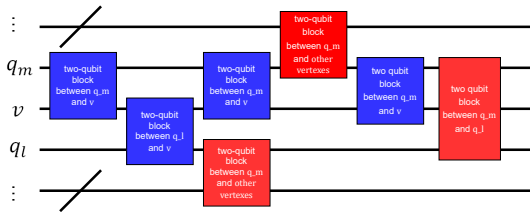


Figure 7: **Example of the computation of S_{ml} .** After ignoring the red blocks, the second and the third blocks between q_m and v can be combined as one block. Thus the sum of the two-qubit block number between is q_m, v and q_l, v is 3.

First, we compute the element of interaction matrix $I_{ml} = aM_{ml} + (1-a)S_{ml}$. We give an example fig. 7(a) of the computation of S_{ml} between q_m and q_l . When only q_m, q_l and v are of interest, we ignore the operations between other vertexes (the red ones), and combine the successive blocks together. At last, we get the sum of the number of the two-qubit blocks in the subcircuits of q_m, v and q_l, v which is $S_{ml} = 2 + 1 = 3$.

Then for every media structure, we compute the element of matrix C , whose elements are the shortest length between v_i, v_j in the media structure.

If no non-media vertex has been allocated on the media struc-

ture, we compute the indicator,

$$E_m = \sum_l I_{ml}, \quad (5)$$

and choose the largest m as the index of the first non-media vertex to allocate. And the location is the vertex with the largest degree under the degree constraint.

Else if there are non-media vertexes have been allocated, we compute another indicator

$$E_m = \sum_{l \in \text{non-media vertexes have been allocated}} I_{ml}, \quad (6)$$

and choose the largest m as the index of next non-media vertex to allocate.

To find the best location for the non-media vertex q_m , we compute

$$s_i = \sum_{j, alloc[j]} C_{ij} I_{alloc[j], m}, \quad (7)$$

for every v_i and the v_i with the smallest s_i will be connected to the q_m , $alloc[i] \rightarrow alloc[i] \cup q_m$. If the degree of v_i break the maximum degree constraint, we repeat the procedure that excluding v_i and choose the v_j with the second smallest s_j until the constraint is met.

Compute the score according to eq. (1) and choose the media structure with the smallest F .

Recovering Subroutine

We sort the *recover_set* from large to small by weight. Then we try to add the edges to the CCG in the order of *recover_set*. If the CCG doesn't violate any constraint after edge addition, then updates the CCG, otherwise, delete the edge we add.

The reason that why the vertex with smaller weight dispersion is more important is as follows. As in fig. 8, in both cases, the vertexes in the middle have the same total weight, while the fig. 8(a) has a smaller weight dispersion. As a result, the weight dispersion of edges that are not connected to the media vertex is smaller. For instance, more weight is concentrated on the one edge weight 7 in fig. 8(a). While in fig. 8(b), the largest weight of edges is only 4, and we can only recover total weight 8 by recovering two edges. Consequently, in fig. 8(a), more weight can be recovered by recovering fewer edges.

Determining the Number of Media Vertexes

We should decide how many high ranking vertexes should be chosen as media vertexes because different circuits have very distinct patterns. E.g., fig. 1(c), is very different from fig. 1(a).

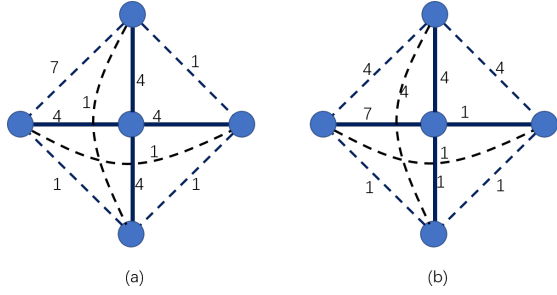


Figure 8: **Example of recovering of different weight dispersion.** (a) The weight dispersion is smaller. So the pruned edges have larger dispersion, (b) vice versa. As a result, more weight are concentrated on fewer pruned edges in (a). We can recover a weight 7 by only recovering one edge, which is impossible in (b).

It is reasonable to choose just one media vertex for fig. 1(a) since almost all weights are concentrated on the edges connected to one vertex. While in fig. 1(c), the weight distribution is uniform. Choosing one media vertex will lose a lot of weight. Therefore, we try N from 1 to the number of CCG vertexes and compute the score $N = \sum_{ml} M_{ml} d_{ml}$, where d_{ml} is the shortest distance between q_m, q_l on the PCG. The smallest score N corresponds to the best choice of the number of media vertexes.

Experiment setup

Benchmarks 158 quantum programs are collected from IBM’s qiskit [48]. These benchmarks cover several important fields and have various sizes for a versatility test of the proposed SPQPD method.

Hardware Model for Comparison We use cross-square structure, triangular lattice structure and the structures in [24] as representatives of lattice-graph structures and compare them with the SPQPD structure.

Circuit Transformation Method The PCG produced by SPQPD is still different from the original CCG. Thus, optimized transformation process are still required. To illustrate the improvement of our method, for all the structures, we use the same Sabre transformation method provided by IBM qiskit [9, 48].

Simulation Tools

The simulation and compilation of quantum algorithms are completed by an open-source software development kit (SDK) IBM qiskit [48].

References

- [1] Bravyi, S., Gosset, D., & König, R. (2018). Quantum advantage with shallow circuits. *Science*, 362(6412), 308-311.
- [2] Bravyi, Sergey, et al. "Quantum advantage with noisy shallow circuits." *Nature Physics* 16.10 (2020): 1040-1045.
- [3] Preskill, John. "Quantum Computing in the NISQ era and beyond." *Quantum* 2 (2018): 79.
- [4] Almudever, Carmen G., et al. "The engineering challenges in quantum computing." *Design, Automation & Test in Europe Conference & Exhibition (DATE), 2017. IEEE, 2017.*
- [5] Cowtan, Alexander, et al. "On the Qubit Routing Problem." 14th Conference on the Theory of Quantum Computation, Communication and Cryptography (TQC 2019), 2019, p. 32.
- [6] Deng, H., Zhang, Y., & Li, Q. (2020). CODAR: A Contextual Duration-Aware Qubit Mapping for Various NISQ Devices. arXiv preprint arXiv:2002.10915.
- [7] Zhou, X., Feng, Y., & Li, S. (2020). A Monte Carlo Tree Search Framework for Quantum Circuit Transformation. arXiv preprint arXiv:2008.09331.

- [8] Niu, Siyuan, et al. "A Hardware-Aware Heuristic for the Qubit Mapping Problem in the NISQ Era." arXiv preprint arXiv:2010.03397 (2020).
- [9] Li, G., Ding, Y., & Xie, Y. (2019, April). Tackling the qubit mapping problem for NISQ-era quantum devices. In *Proceedings of the Twenty-Fourth International Conference on Architectural Support for Programming Languages and Operating Systems* (pp. 1001-1014).
- [10] Pozzi, Matteo G., et al. "Using reinforcement learning to perform qubit routing in quantum compilers." arXiv preprint arXiv:2007.15957 (2020).
- [11] Tannu, Swamit S., and Moinuddin K. Qureshi. "Not all qubits are created equal: a case for variability-aware policies for NISQ-era quantum computers." *Proceedings of the Twenty-Fourth International Conference on Architectural Support for Programming Languages and Operating Systems*. 2019.
- [12] Lin, C. C., Sur-Kolay, S., & Jha, N. K. (2014). PAQCS: Physical design-aware fault-tolerant quantum circuit synthesis. *IEEE Transactions on Very Large Scale Integration (VLSI) Systems*, 23(7), 1221-1234.
- [13] Shafaei, A., Saeedi, M., & Pedram, M. (2014, January). Qubit placement to minimize communication overhead in 2D quantum architectures. In *2014 19th Asia and South Pacific Design Automation Conference (ASP-DAC)* (pp. 495-500). IEEE.
- [14] Wille, R., Lye, A., & Drechsler, R. (2014, January). Optimal SWAP gate insertion for nearest neighbor quantum circuits. In *2014 19th Asia and South Pacific Design Automation Conference (ASP-DAC)* (pp. 489-494). IEEE.
- [15] Lye, A., Wille, R., & Drechsler, R. (2015, January). Determining the minimal number of swap gates for multi-dimensional nearest neighbor quantum circuits. In *The 20th Asia and South Pacific Design Automation Conference* (pp. 178-183). IEEE.
- [16] Wille, R., Burgholzer, L., & Zulehner, A. (2019, June). Mapping quantum circuits to IBM QX architectures using the minimal number of SWAP and H operations. In *2019 56th ACM/IEEE Design Automation Conference (DAC)* (pp. 1-6). IEEE.
- [17] Kole, A., Datta, K., & Sengupta, I. (2016). A Heuristic for Linear Nearest Neighbor Realization of Quantum Circuits by SWAP Gate Insertion Using N -Gate Lookahead. *IEEE Journal on Emerging and Selected Topics in Circuits and Systems*, 6(1), 62-72.
- [18] Siraichi, Marcos Yukio, et al. Qubit allocation. In: *Proceedings of the 2018 International Symposium on Code Generation and Optimization*. 2018. p. 113-125.
- [19] Bhattacharjee, Debjyoti, et al. MUQUT: Multi-constraint quantum circuit mapping on NISQ computers. In: *38th IEEE/ACM International Conference on Computer-Aided Design, ICCAD 2019. Institute of Electrical and Electronics Engineers Inc., 2019. p. 8942132.*
- [20] Venturelli, Davide, et al. Compiling quantum circuits to realistic hardware architectures using temporal planners. *Quantum Science and Technology*, 2018, 3.2: 025004.
- [21] Murali, P. , Linke, N. M. , Martonosi, M. , Abhari, A. J. , Nguyen, N. H. , and Alderete, C. H. . (2019). Full-stack, real-system quantum computer studies: architectural comparisons and design insights.
- [22] Li, G., Ding, Y., & Xie, Y. (2019, April). Tackling the qubit mapping problem for NISQ-era quantum devices. In *Proceedings of the Twenty-Fourth International Conference on Architectural Support for Programming Languages and Operating Systems* (pp. 1001-1014).
- [23] Tan, B., & Cong, J. (2020). Optimality Study of Existing Quantum Computing Layout Synthesis Tools. arXiv preprint arXiv:2002.09783.

- [24] Li, G., Ding, Y., & Xie, Y. (2020, March). Towards efficient superconducting quantum processor architecture design. In Proceedings of the Twenty-Fifth International Conference on Architectural Support for Programming Languages and Operating Systems (pp. 1031-1045).
- [25] Fowler, Austin G., et al. "Surface codes: Towards practical large-scale quantum computation." *Physical Review A* 86.3 (2012): 032324.
- [26] Devitt, S. J., Munro, W. J., & Nemoto, K. (2013). Quantum error correction for beginners. *Reports on Progress in Physics*, 76(7), 076001.
- [27] Jones, N. Cody, et al. "A layered architecture for quantum computing using quantum dots." arXiv preprint arXiv:1010.5022 (2010).
- [28] Chamberland, Christopher, et al. "Topological and subsystem codes on low-degree graphs with flag qubits." *Physical Review X* 10.1 (2020): 011022.
- [29] Egan, Laird, et al. "Fault-Tolerant Operation of a Quantum Error-Correction Code." arXiv preprint arXiv:2009.11482 (2020).
- [30] Boixo, Sergio, et al. "Characterizing quantum supremacy in near-term devices." *Nature Physics* 14.6 (2018): 595-600.
- [31] Arute, Frank, et al. "Quantum supremacy using a programmable superconducting processor." *Nature* 574.7779 (2019): 505-510.
- [32] Krantz, Philip, et al. "A quantum engineer's guide to superconducting qubits." *Applied Physics Reviews* 6.2 (2019): 021318.
- [33] Brink M , Chow J M , Hertzberg J , et al. Device challenges for near term superconducting quantum processors: frequency collisions[C]// 2018 IEEE International Electron Devices Meeting (IEDM). IEEE, 2018.
- [34] Chow, Jerry M., et al. "Simple all-microwave entangling gate for fixed-frequency superconducting qubits." *Physical review letters* 107.8 (2011): 080502.
- [35] Liu, Yu-xi, et al. "Controllable coupling between flux qubits." *Physical review letters* 96.6 (2006): 067003.
- [36] Wang X L , Chen L K , Li W , et al. Experimental Ten-Photon Entanglement[J]. *Physical Review Letters*, 2016, 117(21).
- [37] Monz, Thomas, et al. "14-qubit entanglement: Creation and coherence." *Physical Review Letters* 106.13 (2011): 130506.
- [38] Wallraff, Andreas, et al. "Strong coupling of a single photon to a superconducting qubit using circuit quantum electrodynamics." *Nature* 431.7005 (2004): 162-167.
- [39] Chiorescu, I., et al. "Coherent dynamics of a flux qubit coupled to a harmonic oscillator." *Nature* 431.7005 (2004): 159-162.
- [40] Krinner, Sebastian, et al. "Benchmarking coherent errors in controlled-phase gates due to spectator qubits." *Physical Review Applied* 14.2 (2020): 024042.
- [41] Magesan, E. , & Gambetta, J. M. . (2018). Effective hamiltonian models of the cross-resonance gate.
- [42] Song, Chao, et al. "10-qubit entanglement and parallel logic operations with a superconducting circuit." *Physical review letters* 119.18 (2017): 180511.
- [43] Barends, Rami, et al. "Superconducting quantum circuits at the surface code threshold for fault tolerance." *Nature* 508.7497 (2014): 500-503.
- [44] Simon, Steven H. *The Oxford solid state basics*. OUP Oxford, 2013.
- [45] Chang, Chin-Chih, et al. "Optimality and scalability study of existing placement algorithms." *IEEE Transactions on Computer-Aided Design of Integrated Circuits and Systems* 23.4 (2004): 537-549.
- [46] He, Y., & Bao, F. S. (2020). Circuit routing using monte carlo tree search and deep neural networks. arXiv preprint arXiv:2006.13607.
- [47] Schuch, N., & Siewert, J. (2003). Natural two-qubit gate for quantum computation using the XY interaction. *Physical Review A*, 67(3), 032301.
- [48] Aleksandrowicz, Gadi, et al. "Qiskit: An open-source framework for quantum computing." Accessed on: Mar 16 (2019).
- [49] West, D. B. (1996). *Introduction to graph theory (Vol. 2)*. Upper Saddle River, NJ: Prentice hall.
- [50] Hamed, K. H., & Rao, A. R. (1998). A modified Mann-Kendall trend test for autocorrelated data. *Journal of hydrology*, 204(1-4), 182-196.
- [51] Nielsen, M. A., & Chuang, I. (2002). *Quantum computation and quantum information*.
- [52] Devoret, Michel H., and Robert J. Schoelkopf. "Superconducting circuits for quantum information: an outlook." *Science* 339.6124 (2013): 1169-1174.
- [53] Cross, A. (2018). The IBM Q experience and QISKit open-source quantum computing software. APS, 2018, L58-003.

CODE AND DATA AVAILABLE

The experimental data and the code that support the findings of this study are available from the corresponding author on reasonable request.

AUTHOR CONTRIBUTIONS

B.H.L. designed the method and carried out the numerical calculations. B.H.L. and Y.C.W. analyzed the data and wrote the paper with feedback from all authors. W.C.K. and Q.Z. gave suggestions on the article writing. G.P.G. supervised the project.

COMPETING INTERESTS

The authors declare no competing interests.

ADDITIONAL INFORMATION

Correspondence and request for materials should be addressed to Y.C.W. or G.P.G..

ACKNOWLEDGEMENTS

This work was supported by the National Key Research and Development Program of China (Grant No. 2016YFA0301700) and the Anhui Initiative in Quantum Information Technologies (Grant No. AHY080000).